

Spatially explicit model of the lymphocyte diaspora in influenza-infected lung reveals thresholds on chemokine directed migration

--Manuscript Draft--

Manuscript Number:	PCOMPPBIOL-D-12-01516R1
Full Title:	Spatially explicit model of the lymphocyte diaspora in influenza-infected lung reveals thresholds on chemokine directed migration
Short Title:	Spatial model of directed T cell migration
Article Type:	Research Article
Keywords:	seasonal influenza; avian influenza; 2009 pandemic influenza; agent based model; chemokine directed t cell migration; IP-10; RANTES; bronchial infection
Corresponding Author:	Drew Levin University of New Mexico Albuquerque, NM UNITED STATES
Corresponding Author Secondary Information:	
Corresponding Author's Institution:	University of New Mexico
Corresponding Author's Secondary Institution:	
First Author:	Drew Levin
First Author Secondary Information:	
Order of Authors:	Drew Levin Stephanie Forrest Soumya Banerjee Candice Clay Melanie Moses Frederick Koster
Order of Authors Secondary Information:	
Abstract:	<p>During the primary immune response, clearance of influenza in the lung requires the homing of activated CD8 T cells from regional lymph nodes to infected foci comprising a fraction of the total lung. T cell navigation to infected foci is undirected but emigration into tissue is directed by local cytokine and chemokine production from infected epithelial cells. We focused on the efficiency of local chemokines to induce migration of activated CD8 T cells using a spatially explicit agent-based model (ABM) without constructing a model containing all elements of the immune response.</p> <p>To determine local chemokine production, avian H5N1, seasonal H1N1, and 2009 pandemic influenza strains were used <i>in vitro</i> to induce the secretion of CXCL10 (IP-10) and CCL5 (RANTES) in human bronchial epithelial cells. A differential equation model was fit to empirical chemokine production rates and coupled with published T cell parameters to calibrate the spatial model to test inter-strain variation on T cell recruitment in the lungs. The modeled immune response is unable to clear the pandemic strain due to its high rate of viral production.</p> <p>The spatial nature of the ABM model reveals unique challenges to T cell recruitment not appreciated in standard differential equation models. Infected cells can become isolated in expanding plaques, impeding T cell search, even though the T cells could directionally migrate to low levels of chemokine. A key limitation imposed on T cells is illustrated by their failure to clear the pandemic H1N1 virus after day 6, when T cells became inefficient in large infected foci. This spatially explicit model is consistent with</p>

	efficient T cell recruitment to small infected foci in the lung, but as foci become large T cell search becomes inefficient, thus emphasizing the importance of enhanced control early in infection.
Suggested Reviewers:	<p>Rustom Antia Emory University rustom.antia@emory.edu Dr Antia has a strong background in coupling computational models with experimental immunology.</p> <p>Rob de Boer Utrecht University R.J.DeBoer@uu.nl Has also designed spatially explicit agent-based models to investigate T cell behavior.</p> <p>Joost Beltman Netherlands Cancer Institute j.b.beltman@uu.nl Experience with cell migration and cell-cell interactions, along with experience designing and using computational models.</p> <p>Vitaly Ganusov University of Tennessee vitaly@utk.edu Studies within-host immunity, specifically T cell efficiency during the immune response.</p> <p>Richard Webby St. Jude Children's Research Hospital richard.webby@stjude.org Virologist with a strong background in influenza kinetics.</p> <p>Colleen Jonsson University of Louisville cbjons01@louisville.edu Studies respiratory viruses including 2009 pandemic influenza.</p>
Opposed Reviewers:	<p>Alan Perelson Los Alamos National Laboratory</p> <p>Two of the authors have long-standing collaborations with Alan Perelson, including many co-authored papers, and shared modeling projects.</p>

Dear Editors,

We resubmit this manuscript entitled "Spatially explicit model of the lymphocyte diaspora in influenza-infected lung reveals thresholds on chemokine directed migration" for consideration of publication in PLoS Computational Biology. We would like to thank each of you for giving us the opportunity to improve our paper and resubmit it. We would like to reiterate our thanks to our reviewers for giving us very constructive criticism that we believe has greatly improved the paper. We still feel this work will be of interest to investigators modeling the immune response for the ultimate purpose of improving vaccine design.

This work has not been published elsewhere, and is complementary to a recent publication from our group (H Mitchell, D Levin, et al. J Virol 2011;85(2):1125-1135).

In review we have noticed that our bibliography does not use annotated journal names, which seem to be the standard for PLoS CB. We have *not* changed our bibliography as of yet as it was generated automatically using the Mendeley Desktop suite. If this is an issue, we would be happy to return and reconstruct the references manually.

All authors have read and approved the revised manuscript.

Respectfully yours,

Drew Levin

Stephanie Forrest

Soumya Banerjee

Candice Clay

Melanie Moses

Frederick Koster

Spatially explicit model of the lymphocyte diaspora in influenza-infected lung reveals thresholds on chemokine directed migration (Response to Reviewers)

Drew Levin, Stephanie Forrest, Soumya Banerjee, Candice Clay, Melanie Moses, Frederick Koster

We thank the reviewers for their constructive and insightful comments. The incorporation of the reviewers' comments has greatly improved the paper. We include detailed responses to each comment below.

Reviewer 1

1. The title may be misleading as the model is very simplified from the immunological viewpoint and gives rather a qualitative rather than a quantitative view of the spatial dynamics.

We changed the title by changing the phrase ‘quantifies constraints’ to ‘reveals thresholds’, which we believe more accurately reflects the paper’s main focus.

2. Introduction, p3: It would be interesting to add a general reference to agent-based models (ABM), in particular spatial ABM in immunology and briefly justify the use of an ABM rather than partial differential equations in the present context.

Added reference to Beauchemin 2006 paper that discusses ABM advantages vs. differential equations as well as Bauer 2009. We have added the following sentences to the introduction:

Activated CD8 T cells searching for and homing into infected tissue do so in a spatially complex environment. We therefore used agent-based modeling (ABM) to represent the physical environment of the searching T cell.

3. Computational modeling section: there is no reference to Fig. 1 in the main text. As far as I understand the drawing in Fig. 1, I see 16 branches rather than 14, why?

A reference to Fig. 1 was added to the Model section. The number 14 refers to the depth of the bronchial tree, where each layer represents the bifurcation of a branch. Thus, each level results in the doubling of the total number of pathways. 14 branches refers to $2^{14} = 16,384$ endpoints. The figure simplifies this to 4 layers and thus $2^4 = 16$ endpoints. The figure has been edited to read ‘14 bifurcations’ rather than ‘14 branches’ and the caption was changed to read ‘vascular bifurcations’ for clarity.

4. Acronyms in text and tables should be defined (for example, ODE, FOI, NHBE, ATC, ?).

Acronyms in the text have been either defined or removed. Acronyms in the table are now defined in the caption.

5. Model definition:

- (a) More details concerning the implementation of the ABM need to be given, at least in the supplement: a short description of the spatial arrangement (size of the simulation space, cell arrangement, number of epithelial cells, as well as how T cell movement vs. particle diffusion has been implemented).
- (b) IgM addition is mentioned in section 2.1 of the supplement but not indicated in the main text.
- (c) What happens in this ABM when a free virus particle infects a cell: is it absorbed and does it disappear from the pool of free viruses?

Two new sections were added to the supplement (S1.2, S1.3). One describes details of the general CyCells model environment and the other describes details of the model specific to this paper. These sections address all of the points raised here by the reviewer except IgM. We added a sentence referencing the IgM implementation to the main paper:

IgM is modeled by increasing the viral decay rate by a factor of three after the third day.

6. Materials, p6: the sentence "treatment of the monolayer with protease" is not understandable without reading reference [19] and requires here more explanation.

The description of viral measurement was expanded into two sentences and an explanation of why protease was used was added:

Basal media was collected from previously undisturbed triplicate or quadruplicate wells at 0, 6, 10, 12, 16, 20, 24, 30, 36, 42, 48, and 72 hours after infection, and stored at -80C until assay. Subsequently, apical fluid for virus secretion was collected before and after treatment of the monolayer with protease (Pronase, Sigma) to optimize the collection of infectious virus (Mitchell 2011).

7. Chemokine production, p6:

- (a) **The definition of all the variables and parameters of the ODE model in the supplement (eqs S1) should be added in order to be more self-contained.**

The central differential equation was moved to the beginning of the model section of the main paper and a new table was added with descriptions of every population and parameter.

- (b) **Fig. 3: "8500 pg/mL" is indicated as a measurement threshold for sH1N1. Why is this not also the case for aH5N1 and pH1N1?**

The upper limit applied only to sH1N1 because there were insufficient sample dilutions made and the sample could not be repeated. The sentence in the caption has been rewritten:

sH1N1 IP-10 secretion exceeded measurement accuracy above 8500 pg/mL but these three values (empty red triangles) were not included in the model fitting.

8. T cell sensitivity, p7, top: The sentence "Because multiple T cells ? we hypothesize ? more T cells are not more efficient above a critical threshold" is unclear. Is it not that the probability of apoptosis induction will increase with the T cell number even if the rate of transition from secreting to apoptotic cells does not scale with T cell number?

It is *not* that the probability would increase with additional T cells at the infected epithelial cell in our model. The section has been rearranged to improve clarity. The detail regarding multiple T cells was moved to other sections. We also added two expanded model description sections to the supplement, which we hope clarifies this point.

9. Spatial effects:

(a) p7, bottom: refer also to Fig. S1

A reference to Figure S1 was added.

(b) Figure 6, legend: Can the difference in behaviour for pH1N1 and sH1N1 infections not be explained by the difference in IP-10 production rates (even if small)?

We performed a new model run combining pH1N1 virus and sH1N1 chemokine and found no difference in the infection profile. A sentence was to the spatial effects results section:

Furthermore, increasing chemokine production fails to control the runaway pH1N1 infection (data not shown) suggesting that the effect of high viral production rates dominate low chemokine concentrations in this scenario.

10. Discussion, p10, 2d : reference should also be given to section 2.2 of the supplement where combinations of chemokines are considered.

The Chemokine Directed T cell Search section of the discussion was significantly abbreviated for clarity and removal of information not directly relevant to the modeling exercise. The paragraph in question was removed entirely.

11. Equations:

(a) **Eqs S1: add definition of variables and parameters**

We moved the first equation from the supplement to the main paper to help address the point that the paper is not self-contained. We have added a new table with descriptions and values for each population and parameter of this equation.

(b) **Eqs S2: add definition of t_{rc} and v_{tcell} ; reference to Fig. 1 of the main text should also be given in section 1.2 of the supplement as eqs. S2 relate to the bottom part of this figure.**

These modifications have all been made.

(c) **Section 2.2: does the conclusion that RANTES does not play a significant role for H1N1 infections not simply follows from the fact that IP-10 has a much higher production rate (about 100 times) than RANTES in the H1N1 strains (Table 2, main text)?**

Indeed, it does follow given the assumption that T cells are equally sensitive to each chemokine. The text in S2.2 has been modified to make that assumption clear and to strengthen the conclusion. The following two sentences in particular address the point.

T cell sensitivity depends on receptor density (Desmetz 2006) and this was assumed to be constant. Thus, the chemokines in combination work additively in our model.

This suggests that RANTES does not play a significant role in infections that stimulate an IP-10 response due to the higher production rates of IP-10.

12. Minor points:

- (a) p7, Fig. 5, top row: T cells are barely visible. Could this be improved?

The figure has been enhanced to improve visibility and a note regarding the change has been added to the caption:

Individual cell images for days 5.5 and 7 were enhanced (green dots are enlarged) manually to improve T cell visibility. Thus, individual groups of T cells, which cover only an area of one or two epithelial cells in the model appear larger in the image. Original images available upon request.

- (b) p7, Fig. 6, legend, 5th line: add "more expressing cells than sH1N1".

This has been done.

- (c) p8, line 4: taking the viral production indicated in Table 2, I find 2632 rather than 2643

This was calculated before we rounded to significant digits and has been fixed. (Impressive eye for detail!)

- (d) p9, line 12 from bottom: greater ? than

This sentence has been removed.

- (e) p9, line 3 from bottom: replace "into" by "in"

This has been done.

- (f) Note that some Table and reference numbers have been replaced by question marks in the supplement

These have been fixed.

Reviewer 2

1. Very little detail is given about the agent-based model and how chemokines influence cell migration behavior. The authors cite several papers (4,17,18) but as far as I can see these papers do not provide convincing evidence that chemokines direct migration of effector T cells to the sites of infection (foci of infected cells). In fact, I don't think that there is any evidence of that process. How chemokines direct migration of lymphocytes in tissues is not well understood and the cartoon knowledge of textbooks is mainly applicable to the process of extravasations and may not be used by T cells to find infected cells.

We agree with the reviewer that for the influenza model the evidence for chemokine-directed migration of T cells to infected foci is incomplete. To provide a justification for constructing a math model based on chemokine-directed migration, we have completely rewritten the Introduction in order to thoroughly review the available literature on chemokine function with respect to RNA virus infections. We state that there is no evidence for T cells climbing chemokine gradients, and that this activity has been shown only for neutrophils. However, we feel that the pieces of evidence, taken together, support a reasonable hypothesis for chemokine-directed migration, in addition to extravasation, providing a reasonable justification for the model-building.

2. How you analyze experimental data is unclear. Which equations did you use?

This was a common theme in our reviews. We have made the paper more self-contained by moving the central differential equation to the main paper. We added details of the inner workings of the model to the supplement in two new sections (S1.2 and S1.3). This allows the paper to stand alone from our previous work in Mitchell 2011.

3. Please check parameter values that you provided in Table 1. It appears to several of those are made up and are not really measured in the referenced work.

Table 2 was split into a referenced parameter section and an estimated parameter section to make the distinction clear. We reviewed all of our references and annotated two parameters in Table 2: Apoptosis Time and T Cell Speed as follows:

- Apoptosis time has been rewritten as an estimated parameter and a note has been made that this value is specific to low T cell densities.
- T cell speed has been rewritten as an estimated parameter: *The values were selected to be an order of magnitude faster than those calculated for inside the lymph node (Miller 2003).*

Reviewer 3

A minor comment is that I think it would be interesting to comment in the discussion on the fact that most pathogenic isolates kill the host (in animal models, for sure) presumably before a large CTL infiltration could occur, but that's really not the focus of the manuscript.

While it does not address early mortality in animal hosts, we added a note in the discussion addressing the fact that most humans did not die from pH1N1 infection:

in vivo pH1N1 infection did not usually exhibit a resurgence due to features of the immune response not modeled, specifically antibody and local T cell proliferation

Spatially explicit model of the lymphocyte diaspora in influenza-infected lung reveals thresholds on chemokine directed migration

Drew Levin^{1,*}, Stephanie Forrest¹, Soumya Banerjee¹, Candice Clay², Melanie Moses¹, Frederick Koster^{1,2}

1 Department of Computer Science, University of New Mexico, Albuquerque, NM, USA

2 Lovelace Respiratory Research Institute, Albuquerque, NM, USA

* E-mail: Corresponding drew@cs.unm.edu

Abstract

During the primary immune response, clearance of influenza in the lung requires the homing of activated CD8 T cells from regional lymph nodes to infected foci comprising a fraction of the total lung. T cell navigation to infected foci is undirected but emigration into tissue is directed by local cytokine and chemokine production from infected epithelial cells. We focused on the efficiency of local chemokines to induce migration of activated CD8 T cells using a spatially explicit agent-based model (ABM) without constructing a model containing all elements of the immune response.

To determine local chemokine production, avian H5N1, seasonal H1N1, and 2009 pandemic influenza strains were *in vitro* to induce the secretion of CXCL10 (IP-10) and CCL5 (RANTES) in human bronchial epithelial cells. A differential equation model was fit to empirical chemokine production rates and coupled with published T cell parameters to calibrate the spatial model to test inter-strain variation on T cell recruitment in the lungs. The modeled immune response is unable to clear the pandemic strain due to its high rate of viral production.

The spatial nature of the ABM model reveals unique challenges to T cell recruitment not appreciated in standard differential equation models. Infected cells can become isolated in expanding plaques, impeding T cell search, even though the T cells could directionally migrate to low levels of chemokine. A key limitation imposed on T cells is illustrated by their failure to clear the pandemic H1N1 virus after day 6, when T cells became inefficient in large infected foci. This spatially explicit model is consistent with efficient T cell recruitment to small infected foci in the lung, but as foci become large T cell search becomes inefficient, thus emphasizing the importance of enhanced control early in infection.

Author Summary

Clearance of influenza from the lung depends strongly on the efficiency with which T cells travel from the lymph node to the site of infection. However, T cells in the lung must navigate the large branching bronchial network. This maze-like structure is a challenge for T cell search, and the vast majority of T cells exit the lung without encountering infection. Infected cells produce cytokines and chemokines, which signal T cells to exit the vasculature and enter tissue. We developed an agent-based model to quantify how these molecular signals affect search. Our experimental data show that two chemokines, IP-10 and RANTES, are important for T cell search. We incorporated the data in our spatially explicit model, which allowed us to identify challenges to the search process not obvious in conventional differential equation models. We ran three sets of simulations, using parameters from seasonal influenza, avian influenza, and 2009 pandemic influenza. The simulated immune response contains the first two infections but is unable to contain the highly virulent pandemic strain due to the rapidly expanding plaque size. Direct interventions to improve this T cell search process are unlikely to be effective, and therefore vaccination is required to contain more virulent strains.

Introduction

The adaptive immune response induced during acute influenza A infection is a complex combination of defense mechanisms. Understanding the behavior and interactions of each cellular component may lead to improved vaccines and strategies to control immunopathology. The innate immune response is critical for early control of viral replication, followed by antibody-mediated viral neutralization [1–3]. Complete resolution of influenza pneumonia depends on antigen-specific CD8+ T effector cells [4, 5]. The murine model has been critical in the reductive analysis of each phase and component, permitting temporally explicit descriptions of the induction phase in the regional lymph node [6–8] where recruitment of clonal precursor CD8 T cells is highly efficient [9]. On approximately day 5 after infection, activated CD8 T cells are released from the secondary lymphoid tissue [10] and distributed throughout the body in a process known as the lymphocyte diaspora [11].

The process of recruitment of activated CD8 effector cells to infected sites in the lung is not completely understood. Initial localization and extravasation may depend on a number of inflammatory signals but viral antigen does not appear to induce recruitment into tissue [12]. Effector cells must localize to sites

of viral replication [4], but it is not clear whether cells passing through uninfected lung tissue leave through the pulmonary vein or exit the capillary bed and leave the lung through lymphatic channels. Chemotactic proteins play a major role in recruitment in both acute infections and chronic inflammatory diseases [13,14] where recruited T cells mediate either protection or immunopathology. Infected epithelial cells secrete chemokines [15] and contact with CD8 T cells also triggers secretion [16]. Activated CD8 T effector cells upregulate chemotactic protein receptors, particularly CXCR3 and CCR5 [17,18], responding to their primary ligands CXCL10 (IP-10) and CCL5 (RANTES) respectively.

The consequences of chemotactic ligand-receptor interactions, however, are complex [18,19] and variable in the models studied. For example, in the lymphohochoriomeningitis virus model the CXCR3 receptor mediates T cell recruitment to infected brain and subsequent immunopathology [20,21], while the CCR5 mediates the opposite effect [22]. In contrast, in the West Nile virus model [23] and the dengue model [24], deficiency of IP-10 reduced T cell recruitment to the brain resulting in higher viral burden and increased mortality. In the herpesvirus model, IP-10 was critical in T cell recruitment and disease control in the HSV-2-infected brain [25,26]. In the parainfluenza virus model, CXCR3 receptor is critical in CD4+ T cell migration to the lung [27]. In the influenza A model, initial studies with chemokine receptor knock-out mice obtained mixed results with respect to changing the course of disease [28,29], concluding that redundancy in chemokine signals may confound interpretation. The CXCR3 receptor mediated T cell localization and spared the increased mortality of CCR5 deficiency, but viral clearance was not altered [30]. The CXCR3 receptor also mediates the balance between effector versus memory cell differentiation among recruited CD8 T cells in the lung [31].

Although leukocytes exhibit directional behavior to chemokines [32,33], CD8 T cells have not yet been shown to climb chemokine gradients. Following arrival at the infected site, CD8 T cells secrete cytokines when mononuclear cells are present but in their absence kill infected epithelial cells only by contact cytolysis [34]. Finally the exit of T cells from tissue is tightly regulated to keep effector cells from leaving or dying prematurely [35,36] but effective life-span is unknown.

There are many mathematical models of the entire adaptive response [37–42], filling gaps with reasonable assumptions of cellular behavior in the absence of experimental support. Mathematical and computational models can examine each event in detail and narrow the range of possible behaviors. Here we examine the CD8 T cell diaspora and recruitment to infected lung in detail. Models using ordinary differential equations are able to predict events with temporal fidelity, but lack the ability to examine

the spatial detail [43, 44]. Activated CD8 T cells searching for and homing into infected tissue do so in a spatially complex environment. We therefore used agent-based modeling (ABM) to represent the physical environment of the searching T cell. In the model, CD8 T cells travel in vascular and lymphatic channels during part of their search, and respond to localized inflammatory signals to achieve compartmentalized cell-cell interactions.

We ask how small foci of infected tissue, scattered through a very large space of uninfected tissue, can attract and retain limited numbers of activated CD8 T cells. Our model does not consider important features of tissue immunity such as T cell proliferation, resident T cells, tertiary lymphoid structures, and regulatory interactions with other cell phenotypes [45]. The model does not aim to predict control of viral replication but only to compare simulated outcomes among three influenza strains arising from the efficacy of the chemotactic signals. We use chemotactic protein data from in vitro cultures of bronchial epithelial cells infected with three strains of influenza virus with different replication rates [46] previously described in our laboratory. Using known parameters from the extensive literature on the murine model, we offer several insights on the control of viral replication in lung tissue derived from spatially explicit simulations.

Models

Delay Differential Equation Model

We estimate chemokine production rates by adapting the delay differential equation model of influenza infection described in [46] by adding one new equation to model chemokine production. Initial population sizes and parameter values are taken from the previous study.

$$\begin{aligned}
 \dot{T} &= -\beta TV \\
 \dot{I}_1 &= \beta TV - \beta T[t - \tau_1]V[t - \tau_1] \\
 \dot{I}_2 &= \beta T[t - \tau_1]V[t - \tau_1] - \delta I_2 \\
 \dot{V} &= \frac{p}{1 + eF} I_2 - \beta TV \\
 \dot{F} &= I_1[t - \tau_2] \\
 \dot{C} &= rI[t - \tau_3] - dC
 \end{aligned} \tag{1}$$

Table 1 summarizes population and parameter values and descriptions. Strain-specific values for r

were found by fitting the equations to experimental data (see Results and Table 3).

Computational Modeling

Computational modeling used CyCells [47], a modeling platform for two- or three-dimensional agent-based simulations of the immune response. A simplified model of CD8 T cell activation and recirculation (Fig. 1) was implemented in CyCells (Fig. 2), and simulations measured efficiency of infection clearance under different environmental conditions. The lung was represented as a two-dimensional sheet of healthy epithelial cells. Vasculature was represented as a binary tree with fourteen levels of bifurcations with the origin at the bronchial lymph node complex. Activated T cells descend through the vascular tree until cytokine signal is detected on the local endothelium, at which point they exit the vasculature and follow the chemotactic gradient to the site of infection. T cells that do not encounter cytokine recirculate to the lymph node. When a T cell contacts an infected epithelial cell at the site of infection it induces apoptosis.

The simulation begins when a single cell in the center of the tissue is infected. After the eclipse phase (incubation), the infected cell begins secreting virus and chemokine according to the virus strain and chemokine type. Virus diffuses locally, infecting nearby cells, and continuing the cycle. Chemokine diffuses from secreting cells, creating a circle of stimulation around the infected region. After a five day delay to simulate lymph node stimulation and T cell proliferation, activated T cells exit the lymph node and circulate through the vasculature to the tissue. Because T cells cannot choose their path through the branching network, we assume they arrive in the capillary bed at random locations.

Model Definition

In the model, epithelial cells are stationary and can be in one of five different states: *healthy*, *virus-incubating*, *virus-expressing*, *apoptotic*, and *dead*. *Healthy* cells remain unchanged unless infected by virus. Once infected, the cell transitions from incubating to *expressing*. *Expressing* cells secrete virus and chemokine for approximately 17 hours and then die. *Expressing* cells become *apoptotic* if they encounter activated T cells. Apoptotic cells continue to secrete virus until they die one hour after their transition. *Dead* cells remain inert and do not regenerate over the course of an infection.

T cells have three states. *Circulating* T cells begin to emerge from the lymph node at five days post infection. *Emigrating* T cells arrive at a random location on the lung's surface, wander randomly in the tissue for 10 minutes, and transition to *circulating* in the absence of chemokine. *Circulating* cells

spend six minutes recirculating to the lymph node, transition to *emigrating* and are reintroduced to a new random location in the lung. When a *emigrating* T cell encounters chemokine, it converts to *chemotaxing* and begins following the chemotactic gradient to the source of infection. *Chemotaxing* T cells move continuously up the gradient, inducing apoptosis if they encounter *expressing* epithelial cells. *Chemotaxing* cells decay exponentially with an average lifespan of two hours.

The model contains two kinds of particles: virus and chemokine. Both are produced at constant rates by *expressing* epithelial cells. Virus diffuses through the lung tissue, infecting healthy cells probabilistically according to the local virus concentration. Chemokine diffuses across the tissue but has no direct effect beyond activating T cells. Both particle types decay exponentially. IgM is modeled by increasing the viral decay rate by a factor of three after the third day.

Parameters that are consistent between every model are shown in Table 2. Strain-specific values are shown in Table 3.

Materials

Chemokine secretion: Epithelial cell culture and supernatant collection was performed as described [46]. Briefly, undifferentiated human tracheal epithelial cells (University of Miami) were cultured for 4 weeks to achieve fully differentiated confluent monolayers on collagen-coated transwell inserts, or commercial differentiated human bronchial epithelial cells (EpiAirway Tissue, MatTek Corp., Ashland, MA) used immediately upon receipt, were infected at an MOI of 0.01 with either seasonal H1N1 virus A/New Caledonia/20/99 (sH1N1), the 2009 H1N1 pandemic strain A/California/04/09 (pH1N1), or avian H5N1 virus A/Hong Kong/483/97 (aH5N1) derived from a fatal human infection. Basal media was collected from previously undisturbed triplicate or quadruplicate wells at 0, 6, 10, 12, 16, 20, 24, 30, 36, 42, 48, and 72 hours after infection, and stored at -80C until assay. Subsequently, apical fluid for virus secretion was collected before and after treatment of the monolayer with protease (Pronase, Sigma) to optimize the collection of infectious virus [46]. Quantitative viral culture was performed by standard plaque assay. Quantitative chemokine levels were performed in 30 l aliquots for a panel of chemokines (IL-8, MCP-1, MIP-1 α , MIP-1 β , RANTES, IP-10, eotaxin) and cytokines (interferon-gamma, IL-1 α , IL-1 β , IL-1RA, IL-2, IL-3, IL-4, IL-6, IL-10, IL-12p40, IL-15, IL-17, TNF α) (Luminex Assay, Luminex Corp.) and reported as ng/mL basal media sampled from a total volume of 4 mL. Only IP-10, RANTES, and TNF α showed

increases in production. TNF was ignored as its effects are outside the scope of this paper.

Results

Chemokine production

To provide estimates of chemokine concentrations and secretion rates present in lung tissue, chemokine levels were measured at 4-6h intervals during the first 48 h of infection in wells containing approximately one million human bronchial epithelial cells (Fig. 3). The dynamic viral loads at these intervals in these cultures infected with seasonal H1N1 virus, pandemic H1N1 virus, and avian H5N1 virus have been reported previously [46]. IP-10 concentration increases were observed by 8h post-infection (p.i.), and RANTES by 16h p.i.. To estimate per-cell production rates, we extended the ordinary differential equation (ODE) model of Ref. [46] to represent chemokine production from infected cells (Eq. 1). Model fits (Table 3) were computed for three strains (Fig. 3) using Matlab's `nlinfit` function (Levenberg-Marquardt algorithm). The resulting chemokine production values were used in the CyCells ABM. Best-fit expression rates were similar for all strains except for significantly higher RANTES production in aH5N1. There is no positive correlation between viral production and induced chemokine production across the three strains.

T cell sensitivity to chemokine

The model simulates a chemokine gradient surrounding the infected focus (Fig. 5), based on the calculated per-infected cell secretion rate (Table 3) and known chemical parameters for a 10 kDa protein (Table 2). T cell sensitivity depends on receptor density [48] and this was assumed to be constant.

Because this parameter is unknown, we simulated T cell sensitivity levels ranging over 10 orders of magnitude and found a threshold (Fig. 4) at a concentration of 100 ng/ml (10 ng/ml in aH5N1), beyond which there is no detectable effect on model behavior (model variance is discussed in S2.1.). We then set the sensitivity to 10 ng/mL for all future runs (1 nM concentration assuming a chemokine molecular weight of 10 kDa) [49].

Spatial effects

Spatial effects of viral and chemokine diffusion play an important role in both the spreading and clearing of infections. Free virus particles diffuse from virus secreting cells and infect healthy cells. Chemokine produced by infected cells attracts T cells to the infected cells. Although virus is produced at a higher rate than chemokine, its larger size diffuses much more slowly, while chemokine decays more quickly. These countervailing effects result in similar spatial profiles for the two particle types (Fig. 5). Until day 4 the plaque is dominated by active (incubating and secreting) cells, whereas dead cells are rare. Over time, cells in the plaque's interior die, and active cells form a decreasing proportion of the plaque. T cells arrive at day 5 and begin killing the virus-secreting cells. By day 6 many expressing cells have been eliminated and the plaque is dominated by dead cells. Refer to the videos in Figures S3-S5 to see a representative simulation of seasonal influenza.

In aH5N1, the plaque is dense, allowing T cells to find secreting cells easily, and infection is eliminated. However, secreting cells were not eliminated in either H1N1 simulations (Fig. S1). Secreting cells accounted for at most 10% of the active cell population and less than 1% of the total plaque at 6 days p.i.. T cells still accumulate, but they arrive more slowly than the plaque is growing, leading to lower average T cell killing rate. Further, the regions of concentrated chemokine lag behind the cell and virus spatial layout. It takes time for newly secreting cells to produce chemokine while pockets of high chemokine density are slow to decay. Thus, T cells can fail to detect cellular changes in the plaque. Taken together, the delayed response and low proportion of virus secreting cells prevent T cells from completely clearing the infection. Furthermore, increasing chemokine production fails to control the runaway pH1N1 infection (data not shown) suggesting that the effect of high viral production rates dominate low chemokine concentrations in this scenario.

T cells are unable to kill cells that have not yet presented antigen. At day 5.5, the ratio of secreting cells to the total plaque size is high (Fig. 5-6). By day 7, this ratio is very small for both the pH1N1 and sH1N1 strains, making it much more difficult for searching T cells to find the secreting cells. The high replication rate of pH1N1 enhances this effect (Fig. 6C) and the T cells can control (but not eliminate) the sH1N1 infection. The video in Figure S6 illustrates this event.

A cell infected with pH1N1 produces new virus at the rate of 5.08e-3 PFU/s [46]. That is, in each secreting cell a new viral particle is produced approximately every 200 seconds. Assuming that secretion continues for one hour after apoptosis is initiated, the best a T cell could do is limit production to 18

new viral particles. Thus, T cells alone cannot contain the pH1N1 infection. In contrast, a sH1N1 virus-secreting cell produces a new virus particle every 2,632 seconds, allowing T cells to limit a single infected cell to 1.4 viral particles in the one-hour window. Avian H5N1 virus-secreting cells produce only 0.2 viral particles in the interval after induced apoptosis.

Discussion

Modeling Methodology

The model makes a number of simplifications to and deletions of elements in the innate and adaptive immune response, allowing us to build a tractable model where data was available. Antigen presentation T cell clonal expansion in secondary lymphoid organs is represented solely by the constant rate of emigration of activated CD8 T cells from regional lymph nodes. Virus-specific strain replication rates are represented as constant rates, and virus clearance is also constant. The contribution of IgM antibody clearing free virus is represented as a constant rate, and the class switch to higher affinity antibody mediated by CD4+ T cells is not represented. All of these rates may in fact be time-variable as indicated by data-fitting models [50]. Immigration and contributions of virus-nonspecific immune cells such as macrophages and/or dendritic cells are not represented in our model. Finally, the proliferation of activated T cells in lung tissue is not represented, but is thought to be crucial to the control of lung infection [37]. Thus, our model is not intended to predict clearance of virus from the lung, but to examine the response features that permit CD8 T cells to sense and contact infected target cells.

The use of an ABM has certain advantages over a spatially homogeneous ODE model. An ODE model assumes that any virus particle is capable of infecting any healthy cell. Figure 5 shows that this is clearly not the case for viral adhesion and entry. In fact, most free virus exists on top of infected cells that are no longer candidates for viral binding and fusion. ODE models account for this discrepancy by lowering rates of infection by a constant amount, but this assumes that the proportion of unsuitable virions will always be the same. This is limiting as can be seen in Figure 5 where the early infection has a higher proportion of virus overlapping healthy cells.

Our ABM reveals spatial patterns and dynamics that are absent in differential equation models and difficult or impossible to observe in *in vitro* and *in vivo* systems discussed earlier. Because CD8 T cells find infected cells by presumably climbing a chemokine gradient, we see T cell clustering at local maxima

of chemokine concentration, a possible explanation for why T cells do not increase in effectiveness as their numbers increase. We also see that T cell clustering persists after all virus-secreting cells have been eliminated. The local chemokine maxima takes time to diffuse and decay so that T cells can climb the gradient to a new maximum. Finally, we can see that infected cells are more disperse as infection size grows. Because T cells are clustered they cannot cover the increasing plaque effectively. These spatial observations provide explanations for the pH1N1 resurgence that would be obscured without the visualization tools provided by the ABM (*in vivo* pH1N1 infection did not usually exhibit a resurgence due to features of the immune response not modeled, specifically antibody and local T cell proliferation). The behavior of searching T cells described in this paper can enhance future global immune response models.

Chemokine Directed T Cell Search

The actual quantitative chemokine environment in the infected lung is difficult to estimate for a math model. The hypercytokinemia documented in virulent influenza infections [51] likely does not reflect lung tissue concentrations. Dynamic chemokine concentrations secreted by bronchial epithelial cells *in vitro* depend on infection intensity and cell maturation state [15, 46, 52, 53] but may better approximate actual levels. Interestingly, the attenuation of the type I interferon response by H5N1 strains is not associated with attenuation of chemokine secretion [54]. The model did not incorporate the potential contributions from other chemokines such as CXCL8/IL-8 detected in bronchial cell cultures [55, 56], nor did the model account for chemokines secreted by immigrant macrophages [57] and amplification of epithelial cell secretion by CD8 T cells [16].

A key determinant in the efficiency of chemokine-directed T cell migration towards virus-secreting epithelial cells is the communication distance, defined by the threshold of sufficient chemokine signal required to induce directed motion of the cell up the chemical gradient [58]. The diameter of this gradient generated by a single cell is a function of production rate, decay rate, protein diffusion and the sensitivity threshold. For the threshold of 10 ng/mL and maximal levels of concentration in tissue of 10,000 pg/mL, we calculated the effective communication distance to be approximately 150 microns in our model by simulating a single chemokine producing cell and observing the radius of the resulting chemokine gradient. This calculation is similar to the distance calculated for generic cytokines secreted by a suspended solitary cell [59]. Spatially explicit modeling can provide support for not only communication

distance but also the role of immigrant CD8 T cell proliferation, contribution of resident memory T cells and B cells, and effector cell lifespan.

Acknowledgments

We thank J. Cannon (UNM Pathology and Molecular Genetics & Microbiology), F. Aspert-Boursin (UNM Pathology and Computer Science), S. Jordan (UNM Computer Science and Biology), and G. Bezerra, B. Edwards, and G. Stelle (UNM Computer Science) for suggestions concerning the manuscript, cellular and chemokine behavior, and agent-based modeling.

References

1. Kohlmeier JE, Woodland DL (2009) Immunity to respiratory viruses. *Annual Review of Immunology* 27: 61–82.
2. Joo HM, He Y, Sangster MY (2008) Broad dispersion and lung localization of virus-specific memory B cells induced by influenza pneumonia. *Proceedings of the National Academy of Sciences of the United States of America* 105: 3485–3490.
3. Oslund KL, Baumgarth N (2011) Influenza-induced innate immunity: regulators of viral replication, respiratory tract pathology & adaptive immunity. *Future Virol* 6: 951–962.
4. Cerwenka A, Morgan TM, Harmsen AG, Dutton RW (1999) Migration Kinetics and Final Destination of Type 1 and Type 2 CD8 Effector Cells Predict Protection against Pulmonary Virus Infection. *The Journal of Experimental Medicine* 189: 423–434.
5. Kim TS, Sun J, Braciale TJ (2011) T cell responses during influenza infection: getting and keeping control. *Trends in Immunology* 32: 225–231.
6. Miller MJ, Wei SH, Cahalan MD, Parker I (2003) Autonomous T cell trafficking examined in vivo with intravital two-photon microscopy. *Proceedings of the National Academy of Sciences of the United States of America* 100: 2604–2609.

7. Allan RS, Waithman J, Bedoui S, Jones CM, Villadangos JA, et al. (2006) Migratory dendritic cells transfer antigen to a lymph node-resident dendritic cell population for efficient CTL priming. *Immunity* 25: 153–162.
8. Ingulli E, Funatake C, Jacovetty EL, Zanetti M (2009) Cutting edge: antigen presentation to CD8 T cells after influenza A virus infection. *The Journal of Immunology* 182: 29–33.
9. Van Heijst JWJ, Gerlach C, Swart E, Sie D, Nunes-Alves C, et al. (2009) Recruitment of antigen-specific CD8+ T cells in response to infection is markedly efficient. *Science* 325: 1265–1269.
10. Miao H, Hollenbaugh JA, Zand MS, Holden-Wiltse J, Mosmann TR, et al. (2010) Quantifying the early immune response and adaptive immune response kinetics in mice infected with influenza A virus. *Journal of Virology* 84: 6687–6698.
11. Marshall DR, Turner SJ, Belz GT, Wingo S, Andreansky S, et al. (2001) Measuring the diaspora for virus-specific CD8+ T cells. *Proceedings of the National Academy of Sciences of the United States of America* 98: 6313–6318.
12. Topham DJ, Castrucci MR, Wingo FS, Belz GT, Doherty PC (2001) The role of antigen in the localization of naive, acutely activated, and memory CD8(+) T cells to the lung during influenza pneumonia. *The Journal of Immunology* 167: 6983–6990.
13. Bromley SK, Mempel TR, Luster AD (2008) Orchestrating the orchestrators: chemokines in control of T cell traffic. *Nature immunology* 9: 970–80.
14. Medoff BD, Thomas SY, Banerji A, Wain JC, Zhang H, et al. (2005) Pathogenic T-cell recruitment into the airway in human disease. *Annals Of The New York Academy Of Sciences* 1062: 220–241.
15. Chan MCW, Cheung CY, Chui WH, Tsao SW, Nicholls JM, et al. (2005) Proinflammatory cytokine responses induced by influenza A (H5N1) viruses in primary human alveolar and bronchial epithelial cells. *Respiratory Research* 6: 135.
16. Zhao MQ, Stoler MH, Liu AN, Wei B, Soguero C, et al. (2000) Alveolar epithelial cell chemokine expression triggered by antigen-specific cytolytic CD8(+) T cell recognition. *Journal of Clinical Investigation* 106: R49–R58.

17. Hoji A, Rinaldo CR (2005) Human CD8+ T cells specific for influenza A virus M1 display broad expression of maturation-associated phenotypic markers and chemokine receptors. *Immunology* 115: 239–245.
18. Groom JR, Luster AD (2011) CXCR3 ligands: redundant, collaborative and antagonistic functions. *Immunology and Cell Biology* 89: 207–215.
19. Groom JR, Luster AD (2011) CXCR3 in T cell function. *Experimental Cell Research* 317: 620–631.
20. Christensen JE, Nansen A, Moos T, Lu B, Gerard C, et al. (2004) Efficient T-cell surveillance of the CNS requires expression of the CXC chemokine receptor 3. *Journal of Neuroscience* 24: 4849–4858.
21. Christensen JE, De Lemos C, Moos T, Christensen JP, Thomsen AR (2006) CXCL10 is the key ligand for CXCR3 on CD8+ effector T cells involved in immune surveillance of the lymphocytic choriomeningitis virus-infected central nervous system. *The Journal of Immunology* 176: 4235–4243.
22. De Lemos C, Christensen JE, Nansen A, Moos T, Lu B, et al. (2005) Opposing effects of CXCR3 and CCR5 deficiency on CD8+ T cell-mediated inflammation in the central nervous system of virus-infected mice. *The Journal of Immunology* 175: 1767–1775.
23. Klein RS, Lin E, Zhang B, Luster AD, Tollett J, et al. (2005) Neuronal CXCL10 directs CD8+ T-cell recruitment and control of West Nile virus encephalitis. *Journal of Virology* 79: 11457–11466.
24. Hsieh MF, Lai SL, Chen JP, Sung JM, Lin YL, et al. (2006) Both CXCR3 and CXCL10/IFN-inducible protein 10 are required for resistance to primary infection by dengue virus. *The Journal of Immunology* 177: 1855–1863.
25. Wuest TR, Carr DJJ (2008) Dysregulation of CXCR3 signaling due to CXCL10 deficiency impairs the antiviral response to herpes simplex virus 1 infection. *The Journal of Immunology* 181: 7985–7993.
26. Thapa M, Welner RS, Pelayo R, Carr DJJ (2008) CXCL9 and CXCL10 expression are critical for control of genital herpes simplex virus type 2 infection through mobilization of HSV-specific CTL and NK cells to the nervous system. *The Journal of Immunology* 180: 1098–1106.

27. Kohlmeier JE, Cookenham T, Miller SC, Roberts AD, Christensen JP, et al. (2009) CXCR3 directs antigen-specific effector CD4+ T cell migration to the lung during parainfluenza virus infection. *The Journal of Immunology* 183: 4378–4384.
28. Dawson TC, Beck Ma, Kuziel Wa, Henderson F, Maeda N (2000) Contrasting effects of CCR5 and CCR2 deficiency in the pulmonary inflammatory response to influenza A virus. *The American journal of pathology* 156: 1951–9.

KEY: Dawson2000

ANNOTATION: -*i*, description of the general effect on lung "inflammation" of CCR5 dependent T cell response during influenza infection - CCR5 KO triggers higher mortality rate in influenza infected mice but does not significantly decrease the clearance of the virus (

29. Wareing MD, Lyon AB, Lu B, Gerard C, Sarawar SR (2004) Chemokine expression during the development and resolution of a pulmonary leukocyte response to influenza A virus infection in mice. *Journal of Leukocyte Biology* 76: 886–895.
30. Fadel S, Bromley S, Medoff B, Luster A (2008) CXCR3-deficiency protects influenza-infected CCR5-deficient mice from mortality. *European journal of immunology* 38: 3376–3387.

KEY: Fadel2008

ANNOTATION: These data could be interesting if we want to model both CCL5 and CXCR3 (receptor for CXCL10 or IP-10) because CXCR3 has regulating properties on CCR5 (receptor for CCL5 or RANTES) dependent and/or independent response.

31. Kohlmeier JE, Reiley WW, Perona-Wright G, Freeman ML, Yager EJ, et al. (2011) Inflammatory chemokine receptors regulate CD8(+) T cell contraction and memory generation following infection. *The Journal of Experimental Medicine* 208: 1621–1634.
32. Li Jeon N, Baskaran H, Dertinger SKW, Whitesides GM, Van De Water L, et al. (2002) Neutrophil chemotaxis in linear and complex gradients of interleukin-8 formed in a microfabricated device. *Nature Biotechnology* 20: 826–830.

33. McDonald B, Pittman K, Menezes GB, Hirota SA, Slaba I, et al. (2010) Intravascular danger signals guide neutrophils to sites of sterile inflammation. *Science* 330: 362–366.
34. Hufford MM, Kim TS, Sun J, Braciale TJ (2011) Antiviral CD8+ T cell effector activities in situ are regulated by target cell type. *The Journal of Experimental Medicine* 208: 167–180.
35. Jennrich S, Lee MH, Lynn RC, Dewberry K, Debes GF (2012) Tissue exit: a novel control point in the accumulation of antigen-specific CD8 T cells in the influenza A virus-infected lung. *Journal of Virology* 86: 3436–45.
36. Richter MV, Topham DJ (2007) The alpha₁beta₁ integrin and TNF receptor II protect airway CD8+ effector T cells from apoptosis during influenza infection. *The Journal of Immunology* 179: 5054–5063.
37. Miao H, Hollenbaugh J, Zand M, Holden-Wiltse J, Mosmann T, et al. (2010) Quantifying the early immune response and adaptive immune response kinetics in mice infected with influenza A virus. *Journal of virology* 84: 6687–6698.
38. Saenz RA, Quinlivan M, Elton D, MacRae S, Blunden AS, et al. (2010) Dynamics of influenza virus infection and pathology. *Journal of Virology* 84: 3974–3983.
39. Beltman JB, Marée AFM, De Boer RJ (2007) Spatial modelling of brief and long interactions between T cells and dendritic cells. *Immunology and Cell Biology* 85: 306–314.
40. Handel A, Antia R (2008) A Simple Mathematical Model Helps To Explain the Immunodominance of CD8 T Cells in Influenza A Virus Infections. *Journal of Virology* 82: 7768–7772.
41. Zheng H, Jin B, Henrickson SE, Perelson AS, Von Andrian UH, et al. (2008) How antigen quantity and quality determine T-cell decisions in lymphoid tissue. *Molecular and Cellular Biology* 28: 4040–4051.
42. Lee HY, Topham DJ, Park SY, Hollenbaugh J, Treanor J, et al. (2009) Simulation and Prediction of the Adaptive Immune Response to Influenza A Virus Infection. *Journal of Virology* 83: 7151–7165.
43. Beauchemin C (2006) Probing the effects of the well-mixed assumption on viral infection dynamics. *Journal of Theoretical Biology* 242: 464–477.

44. Bauer AL, Beauchemin CAA, Perelson AS (2009) Agent-based modeling of host-pathogen systems: The successes and challenges. *Information Sciences* 179: 1379–1389.
45. McGill J, Legge KL (2009) Cutting edge: contribution of lung-resident T cell proliferation to the overall magnitude of the antigen-specific CD8 T cell response in the lungs following murine influenza virus infection. *The Journal of Immunology* 183: 4177–4181.
46. Mitchell H, Levin D, Forrest S, Beauchemin Caa, Tipper J, et al. (2011) Higher level of replication efficiency of 2009 (H1N1) pandemic influenza virus than those of seasonal and avian strains: kinetics from epithelial cell culture and computational modeling. *Journal of virology* 85: 1125–35.
47. Warrender C, Forrest S, Koster F (2006) Modeling intercellular interactions in early *Mycobacterium* infection. *Bulletin of Mathematical Biology* 68: 2233–2261.
48. Desmetz C, Lin YL, Mettling C, Portalès P, Rabesandratana H, et al. (2006) The strength of the chemotactic response to a CCR5 binding chemokine is determined by the level of cell surface CCR5 density. *Immunology* 119: 551–61.

KEY: Desmetz2006

ANNOTATION: -; the important factor seems to be the fluctuations of CCR5 (receptor) expression on T cells and less the fluctuations of CCL5 (chemokine) concentration on T cell chemotactic activity. - CCL5 concentration dependent T cell migration (in vitro) -; CCL5 T cell sensitivity ?

49. Gao P, Zhou Xy, Yashiro-ohtani Y, Yang Yf, Sugimoto N, et al. (2003) The unique target specificity of a nonpeptide chemokine receptor antagonist : selective blockade of two Th1 chemokine receptors CCR5 and CXCR3 cated in their migration to sites of inflammation . *Journal of Leukocyte Biology* 73: 273–280.

KEY: Gao2003

ANNOTATION: CCL5 (RANTES) and CXCL10 (IP-10) concentrations inducing T cell chemotaxis (adhesion)

50. Wu H, Kumar A, Miao H, Holden-Wiltse J, Mosmann TR, et al. (2011) Modeling of influenza-specific CD8+ T cells during the primary response indicates that the spleen is a major source of effectors. *The Journal of Immunology* 187: 4474–82.
51. De Jong MD, Simmons CP, Thanh TT, Hien VM, Smith GJD, et al. (2006) Fatal outcome of human influenza A (H5N1) is associated with high viral load and hypercytokinemia. *Nature Medicine* 12: 1203–1207.
52. Chan RWY, Yuen KM, Yu WCL, Ho CCC, Nicholls JM, et al. (2010) Influenza H5N1 and H1N1 Virus Replication and Innate Immune Responses in Bronchial Epithelial Cells Are Influenced by the State of Differentiation. *PLoS ONE* 5: 9.
53. Zeng H, Pappas C, Katz JM, Tumpey TM (2011) The 2009 pandemic H1N1 and triple-reassortant swine H1N1 influenza viruses replicate efficiently but elicit an attenuated inflammatory response in polarized human bronchial epithelial cells. *Journal of Virology* 85: 686–696.
54. Zeng H, Goldsmith C, Thawatsupha P, Chittaganpitch M, Waicharoen S, et al. (2007) Highly Pathogenic Avian Influenza H5N1 Viruses Elicit an Attenuated Type I Interferon Response in Polarized Human Bronchial Epithelial Cells. *Journal of Virology* 81: 12439–12449.
55. Matsukura S, Kokubu F, Noda H, Tokunaga H, Adachi M (1996) Expression of IL-6, IL-8, and RANTES on human bronchial epithelial cells, NCI-H292, induced by influenza virus A. *The Journal of allergy and clinical immunology* 98: 1080–1087.
56. Arndt U, Wennemuth G, Barth P, Nain M, Al-Abed Y, et al. (2002) Release of Macrophage Migration Inhibitory Factor and CXCL8/Interleukin-8 from Lung Epithelial Cells Rendered Necrotic by Influenza A Virus Infection. *Journal of Virology* 76: 9298–9306.
57. Julkunen I, Melén K, Nyqvist M, Pirhonen J, Sareneva T, et al. (2000) Inflammatory responses in influenza A virus infection. *Vaccine* 19 Suppl 1: S32–7.
58. Thelen M, Stein JV (2008) How chemokines invite leukocytes to dance. *Nature Immunology* 9: 953–959.

59. Francis K, Palsson BEO (1997) Effective intercellular communication distances are determined by the relative time constants for cyto/chemokine secretion and diffusion. *Proceedings of the National Academy of Sciences* 94: 12258–12262.
60. Beauchemin C, Forrest S, Koster FT (2006) Modeling Influenza Viral Dynamics in Tissue. *LNCS Artificial Immune Systems* 4163: 23–36.
61. Ganusov VV, De Boer RJ (2008) Estimating in vivo death rates of targets due to CD8 T-cell-mediated killing. *Journal of Virology* 82: 11749–11757.
62. Banerjee S, Moses M (2010) Scale invariance of immune system response rates and times: perspectives on immune system architecture and implications for artificial immune systems. *Swarm Intelligence* 4: 301–318.
63. Banerjee S, Levin D, Moses M, Koster F, Forrest S (2011) The Value of Inflammatory Signals in Adaptive Immune Responses. *ICARIS* 6825: 1–14.
64. Wu CFJ (1986) Jackknife, Bootstrap and Other Resampling Methods in Regression Analysis. *Annals of Statistics* 14: 1261–1295.

Figure Legends

Figure 1. Model of T cell search. Activated T cells originate in the lymph node and enter the bloodstream after which they randomly navigate through 14 vascular bifurcations of the bronchial network. Upon reaching a capillary, T cells exit into tissue if cytokine signal is present. In the absence of signal, the T cell recirculates either through the lymph network or through the pulmonary vein back to the top of the network.

Figure 2. Visual representation of the model. Healthy epithelial cells infected by virus begin secreting virus after the incubation delay. Activated T cells traverse the bronchial vascular network and may be recruited by inflammatory cytokine. Chemotaxing T cells climb the chemokine gradient and induce apoptosis in infected cells. Solid arrows represent a cell state transition from one behavior to another. Dashed arrows display the mechanism used to induce a transition. Dotted arrows indicate the production of new virus.

Figure 3. Empirical viral and cytokine titers for three strains of influenza: Avian H5N1, Seasonal sH1N1, and Pandemic pH1N1. Viral titer (blue circles) is in PFU/mL, and IP-10 (red triangle) and RANTES (green square) are shown in ng/mL. sH1N1 IP-10 secretion exceeded measurement accuracy above 8500 pg/mL but these three values (empty red triangles) were not included in the model fitting. Dashed lines show model fits to IP-10 and RANTES data. Human bronchial epithelial cells were infected at an MOI of 0.01 with one of the three strains of influenza. Apical fluid for viral secretion and basal media for chemokine secretion was collected at the given time intervals post infection. Viral culture was performed by a standard plaque assay and chemokine levels were measured using 30 l aliquots for a panel of 17 chemokines and cytokines (not shown).

Figure 4. Varying T cell sensitivity to chemokine. H5N1 model results use RANTES only, and sH1N1 and pH1N1 use both IP-10 and RANTES. Total number of incubating, secreting and apoptotic cells are plotted for each infection. The sensitivity value specifies the minimum level of chemokine concentration required for T cells to detect it.

Figure 5. Simulated sH1N1 infection. Screenshots from day 4, day 5.5, and day 7. The top row shows the spreading focus of infection through the color coding of individual cells: healthy cells in uninfected tissue (gray), virus-incubating cells (yellow), virus-secreting cells (orange), apoptotic cells (red), dead cells (brown), and T cells arriving at day 5 (green). Free virus and chemokine particles are represented by compartmentalized concentrations of mols/mL and ng/mL. Individual cell images for days 5.5 and 7 were enhanced (green dots are enlarged) manually to improve T cell visibility. Thus, individual groups of T cells, which cover only an area of one or two epithelial cells in the model appear larger in the image. Original images available upon request.

Figure 6. Simulated infections of aH5N1, sH1N1, and pH1N1. Plotted values: total plaque size (blue), number of virus incubating cells (yellow), number of virus secreting cells (green), and T cells (red). T cells clear secreting and incubating cells in aH5N1, fail to clear incubating cells in sH1N1, and fail to clear either type of infected cell in pH1N1. The number of expressing cells (green) after day 5 differs markedly among the three strains indicating that the T cells have differing success at controlling the infection.

Tables

Population	Description	Initial Value
T	Healthy target epithelial cells	1,000,000
I_1	Virus-incubating cells	0
I_2	Virus-secreting cells	0
V	Free virus particles	10,000
F	Interferon quantity	0
C	Chemokine quantity (ng/mL)	0
Parameter	Description	Value
β	Viral infection rates	
	Avian	5.3e-7 (PFU·h) ⁻¹
	Seasonal	6.1e-7 (PFU·h) ⁻¹
	Pandemic	2.7e-6 (PFU·h) ⁻¹
p	Viral production rates	
	Avian	0.20 (PFU/h)
	Seasonal	1.4 (PFU/h)
	Pandemic	18.3 (PFU/h)
e	Interferon strengths	
	Avian	1.0e-8
	Seasonal	1.6e-6
	Pandemic	3.4e-3
τ_2	Interferon production delays	
	Avian	21.5 (h)
	Seasonal	23.6 (h)
	Pandemic	21.0 (h)
δ	Virus-secreting cell decay rate	0.6 (h ⁻¹)
d	Chemokine decay rate	1.386 (h ⁻¹)
τ_1	Viral incubation time	10 (h)
τ_3	Chemokine production delays	
	IP-10	8 (h)
	RANTES	16 (h)

Table 1. All parameters and populations are taken from [46] except for C , d , and τ_3 . The value chosen for d corresponds to a 30 minute half-life and values for τ_3 were take from the observed chemokine data (Fig. 3). Interferon (F) is an abstracted unitless quantity and thus e is a unitless multiplier.

Referenced Parameters	Value	Source
Viral Diffusion in Airway	.0318 $\mu\text{m}^2/\text{s}$	[60]
Viral Decay in Airway	1/day	[42]
Chemokine Diffusion Rate	.318 $\mu\text{m}^2/\text{s}$	[60]
Incubation Time	10 hours	[46]
T cell Production Rate	777/hour	[37]
Blood Circulation Time	6 minutes	[62]
Search Time In Chemokine-Free Tissue	10 minutes	[62]
T Cell Sensitivity to Chemokine	10 ng/mL	[49]
Onset of ATC [‡] Lymph Node Exit	5 days	[63]
Estimated Parameters	Value	Footnote
Chemokine Decay Rate	$3.8508 \cdot 10^{-4}/\text{s}$	1
Infection Sensitivity Rate	2 hour/virion	2
Expression Time	16.7 hours	[46] ³
T Cell Expected Kill Time	10 min	4
Apoptosis Time	60 minutes	[61] ⁵
Epithelial Cell Radius	25 μm	6
T Cell Age (at FOI*)	2 hours	7
T Cell Age (in Blood)	3 days	7
T Cell Speed (Search)	30 $\mu\text{m}/\text{s}$	[6] ⁸
T Cell Speed (Chemotaxis)	3 $\mu\text{m}/\text{s}$	[6] ⁸
IgM Strength	Viral decay of 3/day	9

Table 2. Values are taken from literature if possible, otherwise estimate values are estimated as follows. 1) Corresponds to a 30 minute half-life. 2) Epithelial cells are infected at a probabilistic rate such that the expected time for infection in the presence of a single virion is 2 hours. This scales linearly with the number of virions in the cell's vicinity. 3) Chosen as a plausible median time (1,000 minutes) between 6 hours and 24 hours. 4) T cells induce apoptosis in nearby virus-secreting epithelial cells at a probabilistic rate such that the expected time to induce apoptosis is 10 minutes. This rate does not scale with T cell numbers. 5) Calculated for low T cell densities. 6) The mean surface area of the epithelial cell available for virus contact and entry includes cilia and the radius is estimated to be 25 microns. 7) Chosen to be at the lower end of biologically plausible values because increased T cell counts are shown not to affect the model behavior. 8) The values were selected to be an order of magnitude faster than those calculated for inside the lymph node. 9) IgM presence is abstracted by increasing viral decay by a factor of three. [‡]Activated T Cell. *Focus of Infection.

Strain	IP-10 Production ($pg/s \cdot cell$)	RANTES Production ($pg/s \cdot cell$)	Viral Production ($PFU/s \cdot cell$)
Avian H5N1	2.0e-4 8.4e-5 — 4.2e-4	1.3e-5 7.9e-6 — 1.9e-5	5.4e-5 4.4e-5 — 3.7e-4
Seasonal H1N1	1.8e-4 1.2e-4 — 3.0e-4	8.9e-7 4.8e-7 — 1.6e-6	3.8e-4 2.8e-4 — 1.5e-3
Pandemic H1N1	8.7e-5 1.7e-5 — 7.1e-4	4.3e-6 5.0e-7 — 3.5e-5	5.1e-3 2.8e-3 — 5.3e-3

Table 3. Strain-specific model parameters. Small text values show 95% confidence intervals resulting from 1,000 bootstrapping runs for each parameter [64]. Viral production values are taken from [46].

**Lymph
Recirculation**

**Lymph
Node**

**Venous
Recirculation**

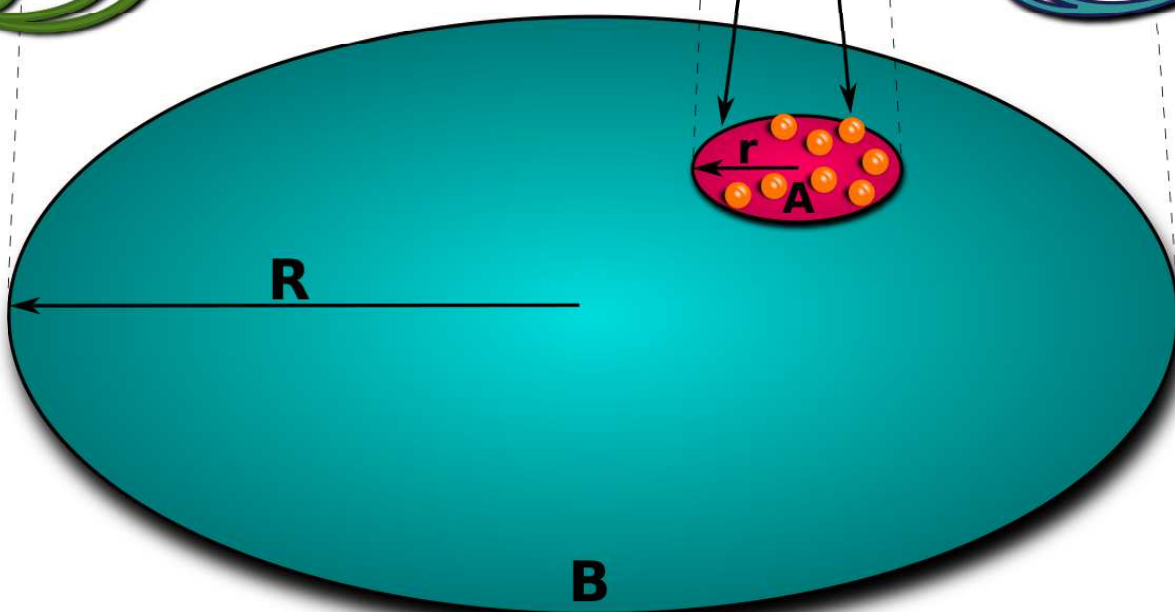
T-cell

**Lung
Vascular
Network**

14 Branches



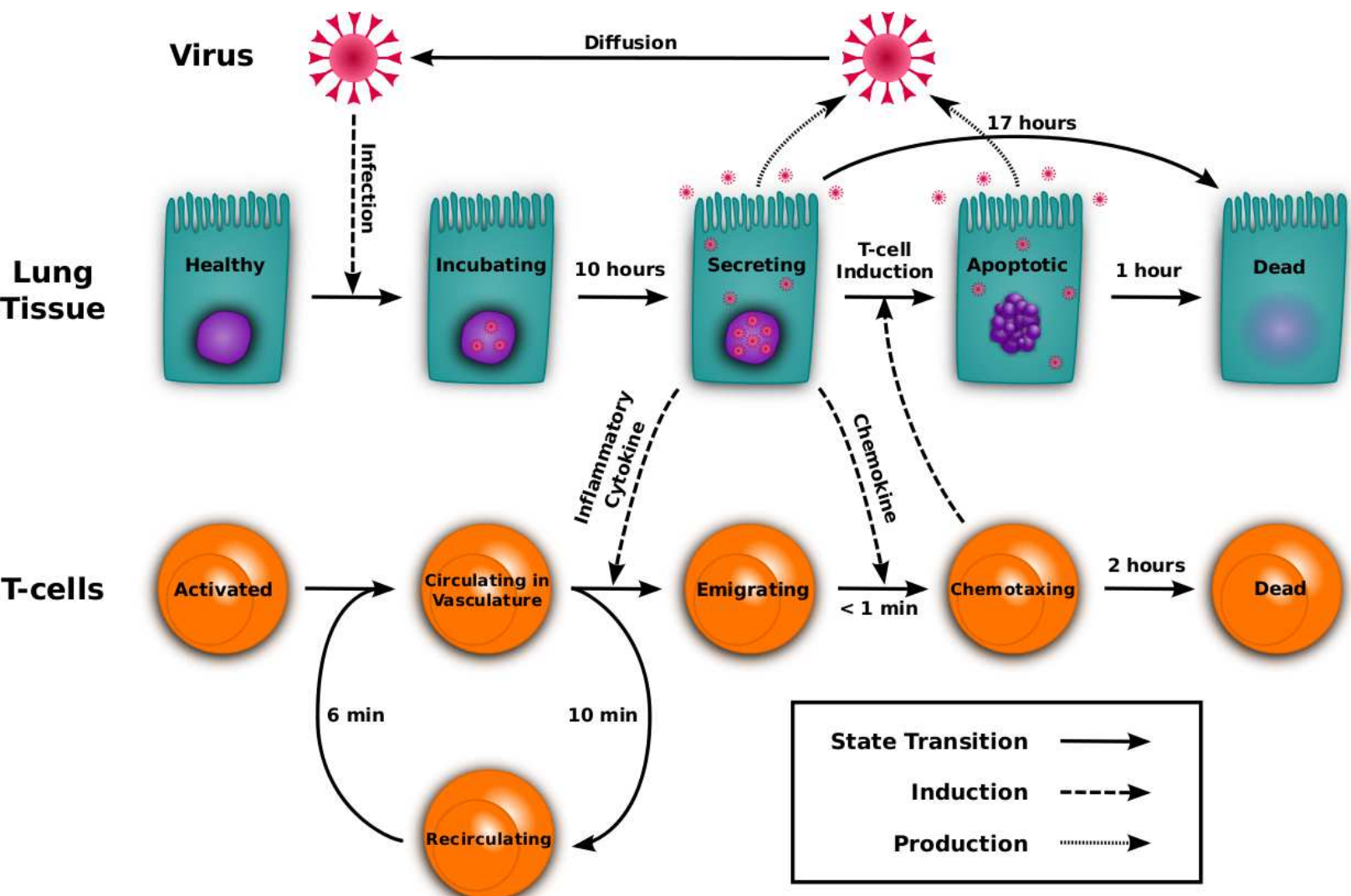
r
 A



**Lung
Tissue**

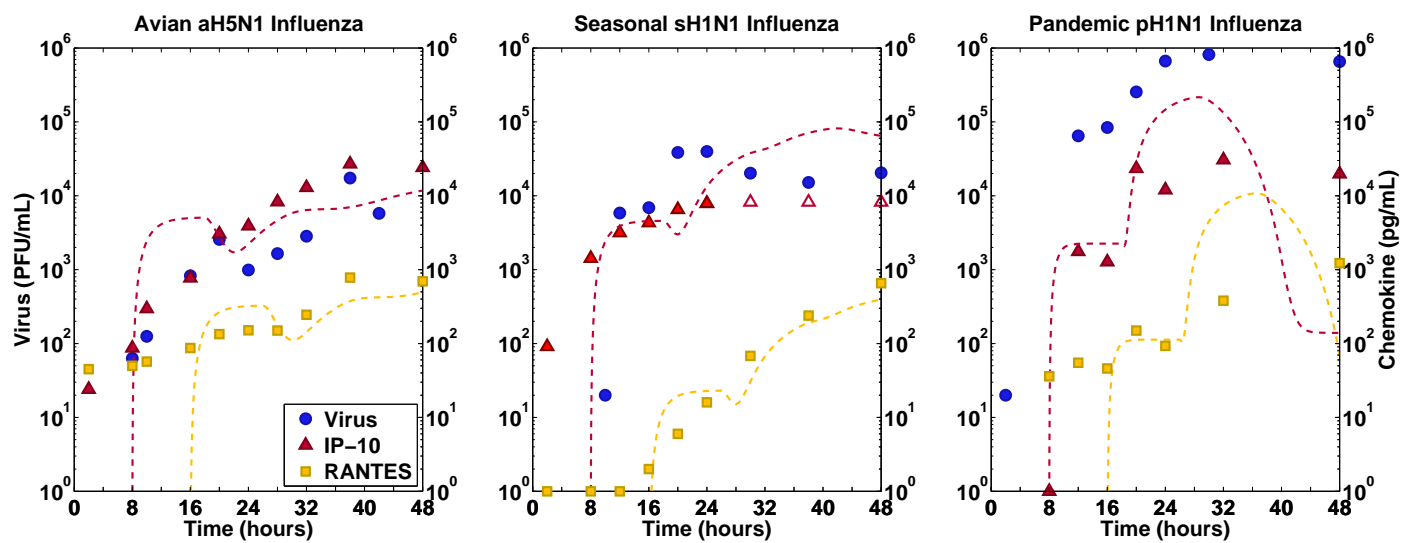
Figure

[Click here to download Figure: ModelChart.eps](#)



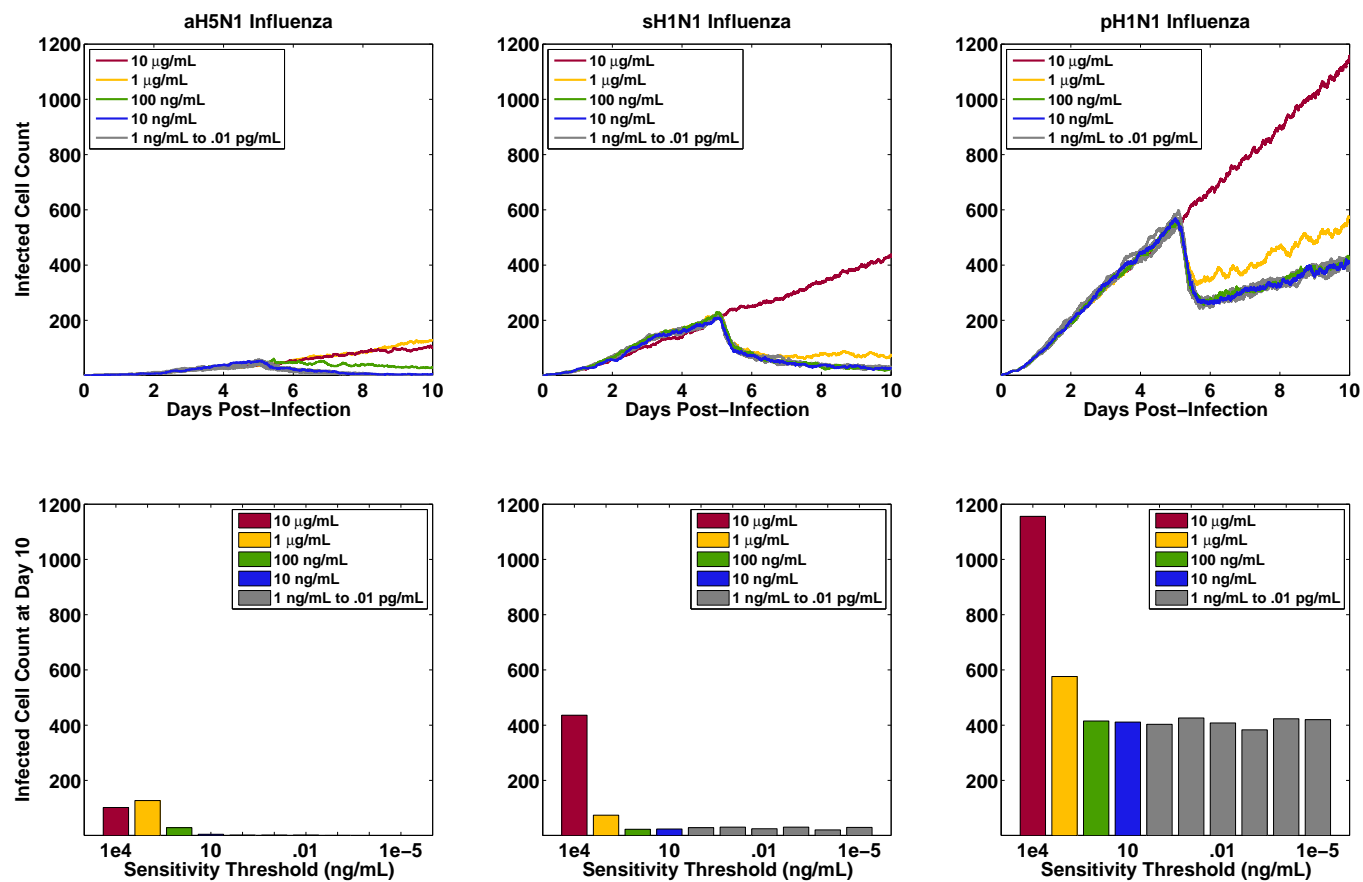
Figure

[Click here to download Figure: data.eps](#)



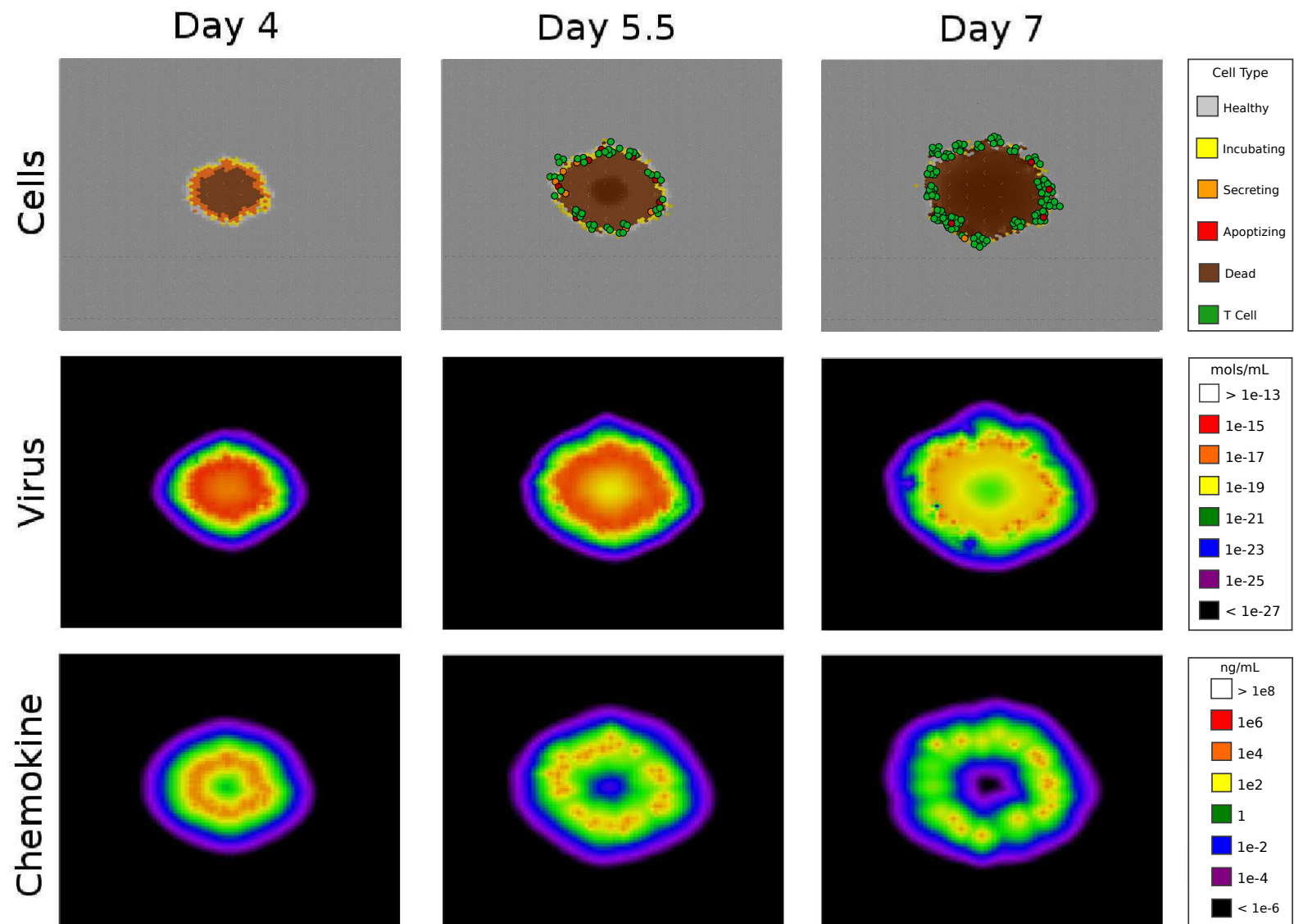
Figure

[Click here to download Figure: sensitivity.eps](#)



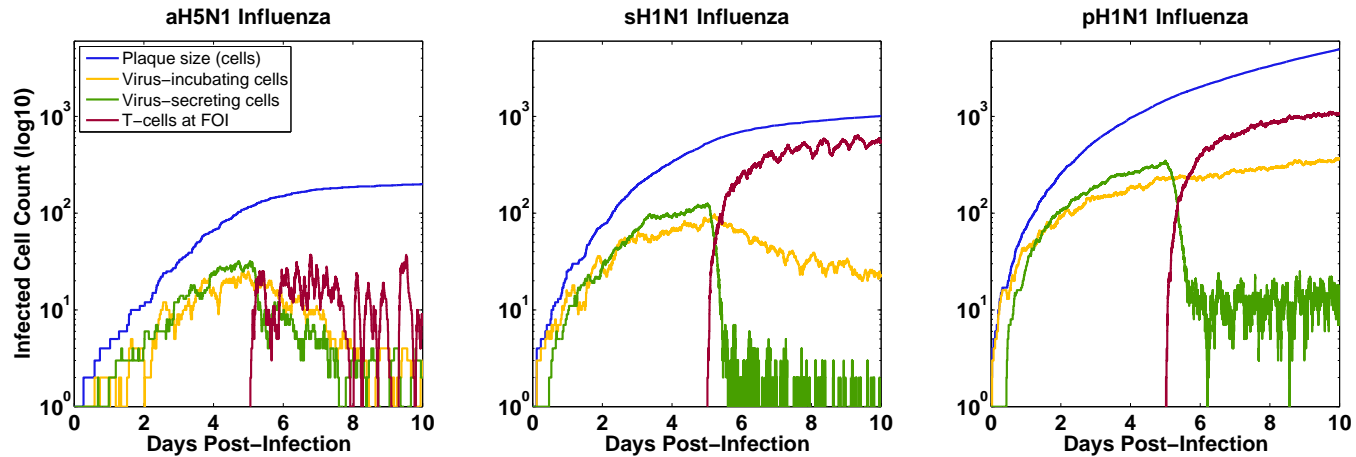
Figure

[Click here to download Figure: cycells.eps](#)



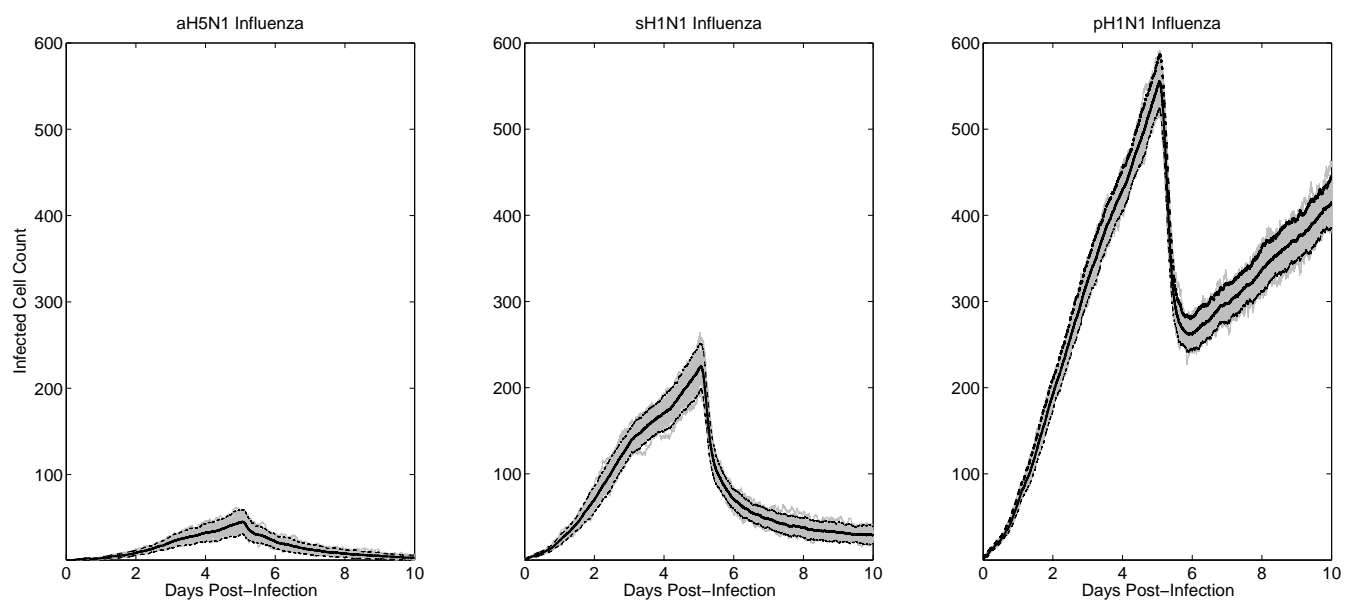
Figure

[Click here to download Figure: plaquesize.eps](#)



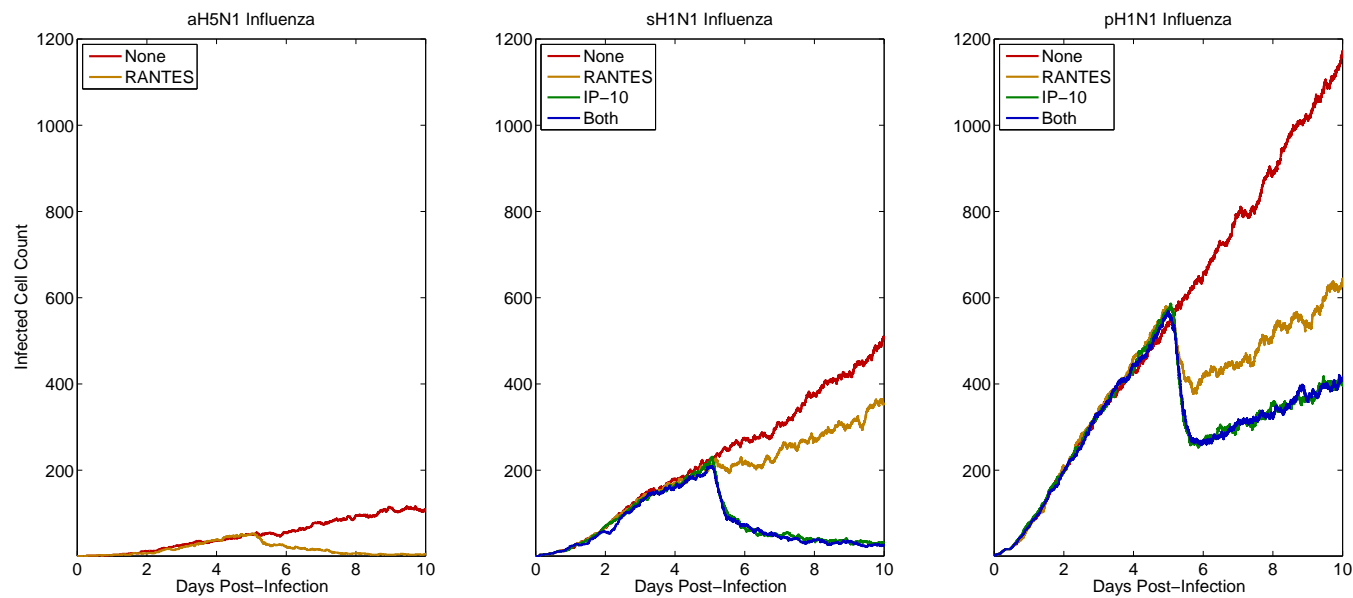
Figure

[Click here to download Figure: variance.eps](#)



Figure

[Click here to download Figure: chemokine.eps](#)



Supporting Information

[Click here to download Supporting Information: chemokine_supplement.pdf](#)

Supporting Information - Compressed/ZIP File Archive

[Click here to download Supporting Information - Compressed/ZIP File Archive: fig_s3.zip](#)

Supporting Information - Compressed/ZIP File Archive

[Click here to download Supporting Information - Compressed/ZIP File Archive: fig_s4.zip](#)

Supporting Information - Compressed/ZIP File Archive

[Click here to download Supporting Information - Compressed/ZIP File Archive: fig_s5.zip](#)

Supporting Information - Compressed/ZIP File Archive

[Click here to download Supporting Information - Compressed/ZIP File Archive: fig_s6.zip](#)

LaTeX Source File (TEX file)

[Click here to download LaTeX Source File \(TEX file\): chemokine_main.tex](#)

LaTeX Source File (TEX file)

[Click here to download LaTeX Source File \(TEX file\): chemokine_supplement.tex](#)

LaTeX Bibliography (BIB file)

[Click here to download LaTeX Bibliography \(BIB file\): references.bib](#)